

Supplementary Materials for

Wireless, battery-free optoelectronic systems as subdermal implants for local tissue oximetry

Hao Zhang, Philipp Gutruf, Kathleen Meacham, Michael C. Montana, Xingyue Zhao, Antonio M. Chiarelli, Abraham Vázquez-Guardado, Aaron Norris, Luyao Lu, Qinglei Guo, Chenkai Xu, Yixin Wu, Hangbo Zhao, Xin Ning, Wubin Bai, Irawati Kandela, Chad R. Haney, Debashis Chanda, Robert W. Gereau IV, John A. Rogers*

*Corresponding author. Email: jrogers@northwestern.edu.

Published 8 March 2019, *Sci. Adv.* **5**, eaaw0873 (2019)

DOI: 10.1126/sciadv.aaw0873

The PDF file includes:

- Fig. S1. Scheme of the fabrication steps of the dual-layered wireless, battery-free oximeters.
- Fig. S2. Scheme of wireless oximeters with different designs of injectable filaments.
- Fig. S3. Optical images of the tip end of injectable filaments of wireless oximeters.
- Fig. S4. Photographs of wireless oximeters with battery-powered electronic modules.
- Fig. S5. Photograph of a battery-free, fully implantable, wireless oximeter on a balance.
- Fig. S6. Ratio of extinction coefficients of HbO₂ and Hb.
- Fig. S7. Scheme of the epitaxial stack of GaAs wafers used for the fabrication of μ -IPDs.
- Fig. S8. Scheme and pseudocolored SEM image of GaAs-based μ -IPDs.
- Fig. S9. Characterizations of μ -IPD and μ -ILEDs.
- Fig. S10. Monte Carlo simulation results.
- Fig. S11. Scheme of the experimental arena circumflexed with antenna for wireless power supply.
- Fig. S12. Transmittance spectra of mouse scalp collected by a fiber optic spectrometer.
- Fig. S13. Fluctuations in output signals ($\Delta I/I$) of the wireless, battery-free oximeters over time.
- Fig. S14. Absorption spectra of five artificial blood solutions with various combinations of oxyhemoglobin, deoxyhemoglobin, and metHb.
- Fig. S15. Raw data of rStO₂ collected by wireless, battery-powered oximetry implants in the tissue region near femoral artery of anesthetized rats.
- Fig. S16. Surgical steps of the subdermal implantation of wireless, battery-free oximeters in mouse brain.
- Fig. S17. Wireless oximetry data on mice with subdermally implanted, battery-free devices in the brain.
- Fig. S18. Photographs of freely moving mice with brain-implanted oximeter filaments with connectors for the integration with battery-powered electronics.
- Fig. S19. Weight changes of three mice after subdermal brain surgery with wireless, battery-free oximetry implants.

Table S1. Data transmission of the wireless, battery-free oximeters before and after subdermal implantation.

Legend for movie S1

Other Supplementary Material for this manuscript includes the following:

(available at advances.sciencemag.org/cgi/content/full/5/3/eaaw0873/DC1)

Movie S1 (.mp4 format). A wireless, battery-free, fully implantable oximeter with illuminating μ -ILEDs.

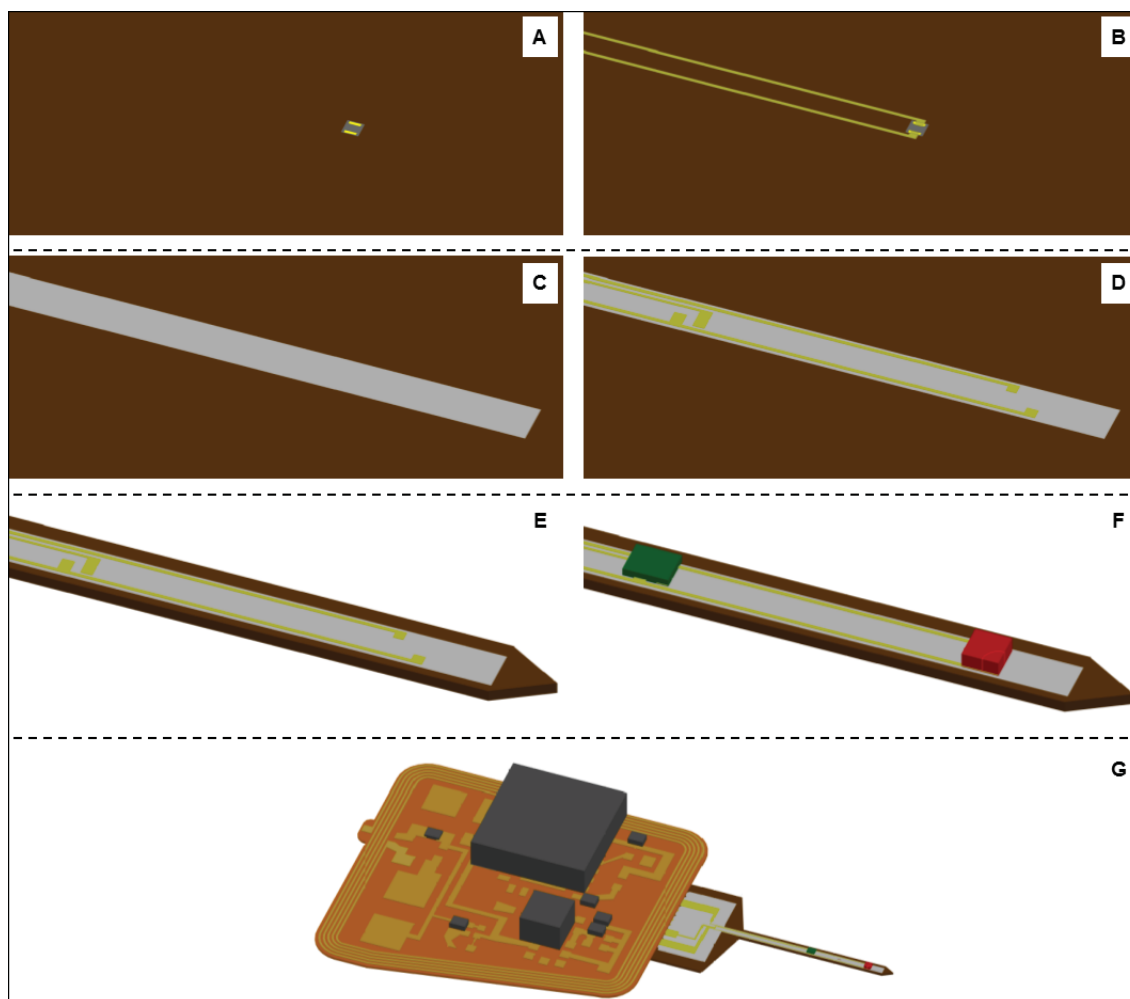


Fig. S1. Scheme of the fabrication steps of the dual-layered wireless, battery-free oximeters.

(A) Micro-transfer printing of a μ -IPD on a 75 μm -thick PI substrate; (B) Deposition of first layer of Au/Cu interconnects for the μ -IPD; (C) Photopatterning of a 7 μm -thick SU-8 separation layer; (D) Deposition of the second layer of Au/Cu interconnects for the μ -ILEDs; (E) Cutting out the shape of injectable filaments by UV laser; (F) Micro-transfer printing and soldering of the μ -ILEDs; (G) Integration of the injectable filament and electronic module into a complete embodiment via low temperature reflow soldering. Note only part of the electronic components are shown in (G).

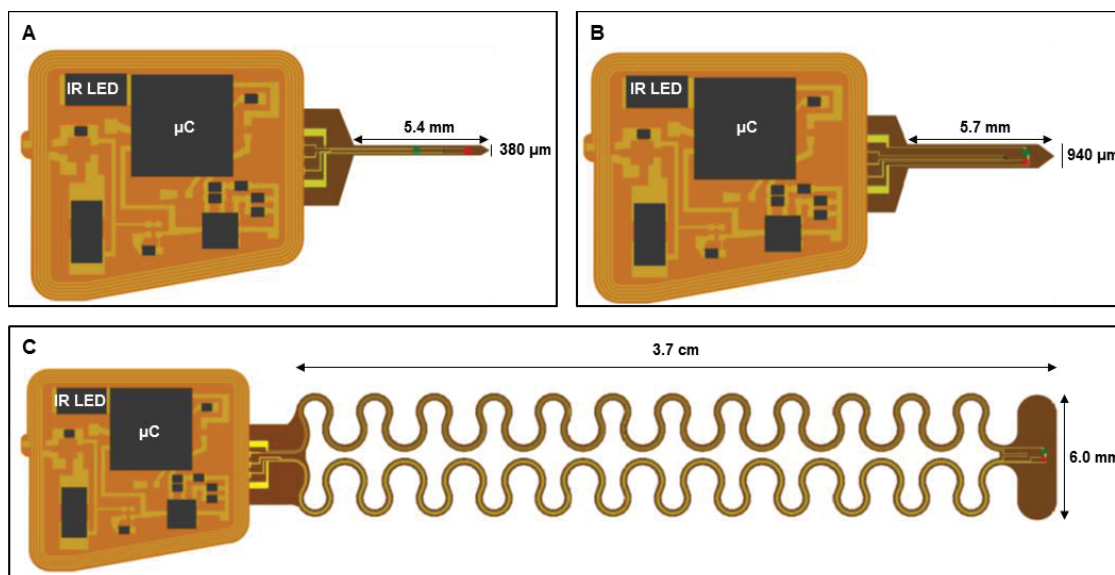


Fig. S2. Scheme of wireless oximeters with different designs of injectable filaments. (A) The dual-layered design with a sub-400 μm width for deep brain rStO₂ sensing of mice. The SU-8 separation layer is omitted for clarity; (B) The single-layered design for highly localized rStO₂ sensing in other tissue regions; (C) The stretchable design with serpentine-shaped interconnects.

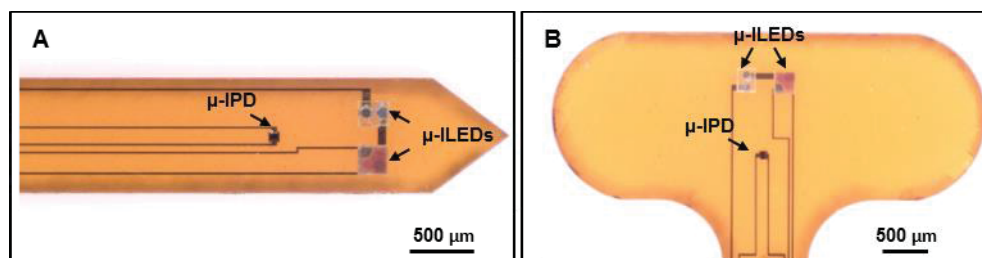


Fig. S3. Optical images of the tip end of injectable filaments of wireless oximeters. (A) Single-layered and (B) stretchable designs.

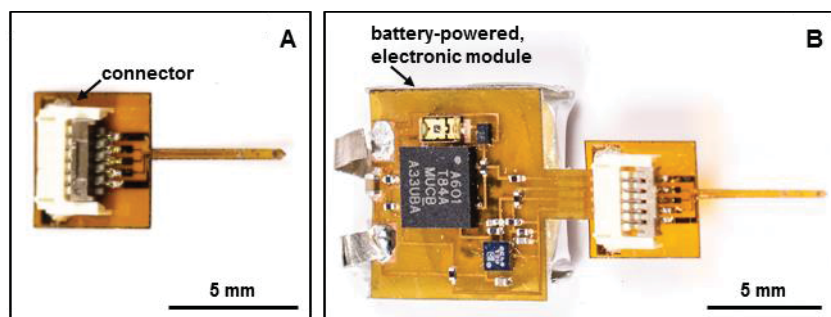


Fig. S4. Photographs of wireless oximeters with battery-powered electronic modules. (A)

The filamentary sensing module with a back-flip connector; **(B)** A complete device embodiment with the detachable, battery-powered electronic module. (Photo credit: Philipp Gutruf, Northwestern University)



Fig. S5. Photograph of a battery-free, fully implantable, wireless oximeter on a balance.

(Photo credit: Philipp Gutruf, Northwestern University)

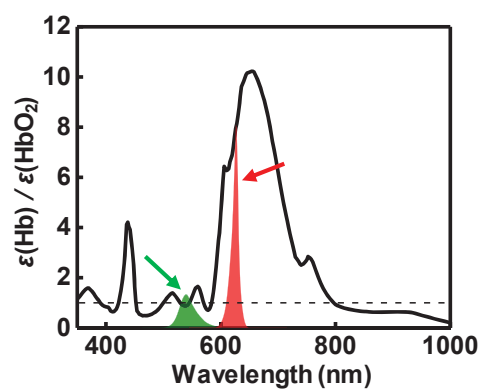


Fig. S6. Ratio of extinction coefficients of HbO₂ and Hb. Green and red shaded areas indicate the emission spectra of green and red μ -ILEDs, respectively. The dashed line corresponds to $\varepsilon(\text{Hb}) = \varepsilon(\text{HbO}_2)$.

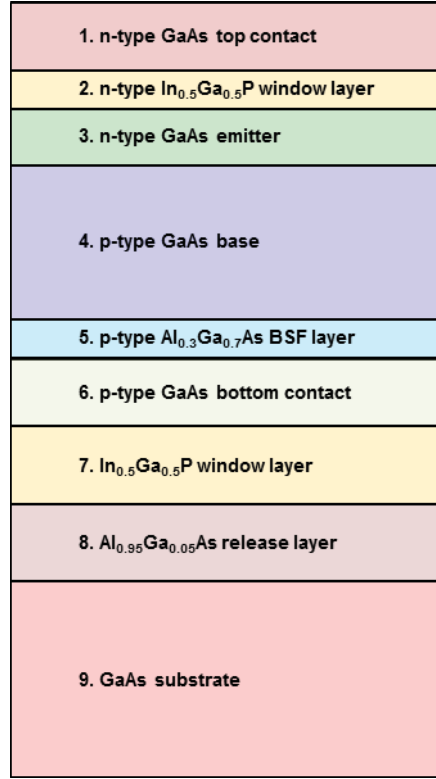


Fig. S7. Scheme of the epitaxial stack of GaAs wafers used for the fabrication of μ -IPDs. 1. n-type GaAs top contact, 100 nm, Te-doped, $>1 \times 10^{19} \text{ cm}^{-3}$ and 100 nm, Si-doped, $\sim 2 \times 10^{18} \text{ cm}^{-3}$; 2. n-type $\text{In}_{0.5}\text{Ga}_{0.5}\text{P}$ window layer, 25 nm, Si-doped, $2 \times 10^{18} \text{ cm}^{-3}$; 3. n-type GaAs emitter layer, 100 nm, Si-doped, $2 \times 10^{18} \text{ cm}^{-3}$; 4. p-type GaAs base layer, 2500 nm, Zn-doped, $1 \times 10^{17} \text{ cm}^{-3}$; 5. p-type $\text{Al}_{0.3}\text{Ga}_{0.7}\text{As}$ back surface field (BSF) layer, 100 nm, Zn-doped, 5×10^{18} to $1 \times 10^{19} \text{ cm}^{-3}$; 6. p-type GaAs bottom contact layer, 300 nm, Zn-doped, $5 \times 10^{19} \text{ cm}^{-3}$; 7. $\text{In}_{0.5}\text{Ga}_{0.5}\text{P}$ window layer, 700 nm, no doping; 8. $\text{Al}_{0.95}\text{Ga}_{0.05}\text{As}$ release layer, 500 nm; 9. GaAs substrate.

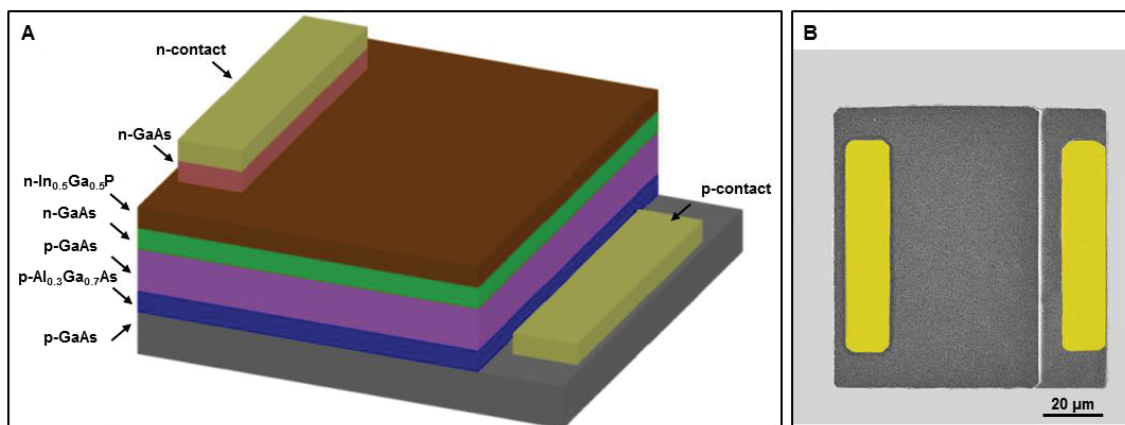


Fig. S8. Scheme and pseudocolored SEM image of GaAs-based μ -IPDs. The n- and p-contacts in (B) are shown in yellow color.

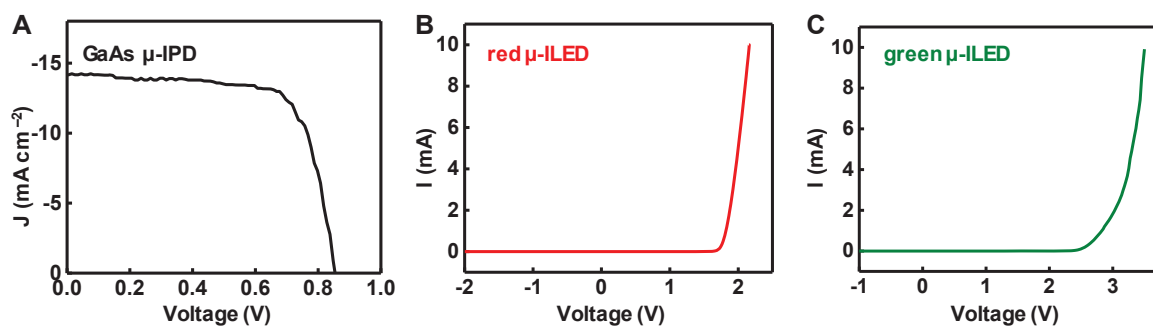


Fig. S9. Characterizations of μ -IPD and μ -ILEDs. (A) Current density versus voltage (J–V) curve of a GaAs μ -IPD under AM 1.5 G (100 mW cm^{-2}) illumination. (B, C) Current versus voltage (I–V) curves of red and green μ -ILEDs.

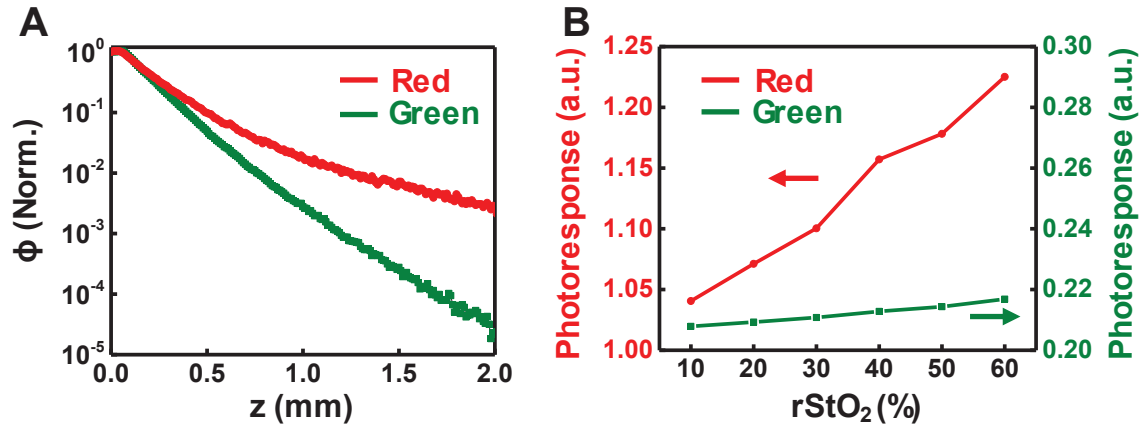


Fig. S10. Monte Carlo simulation results. (A) Normalized light intensities from red and green μ -ILEDs along z -axis and (B) Photoresponses of μ -IPD in response to red and green μ -ILEDs versus $r\text{StO}_2$.

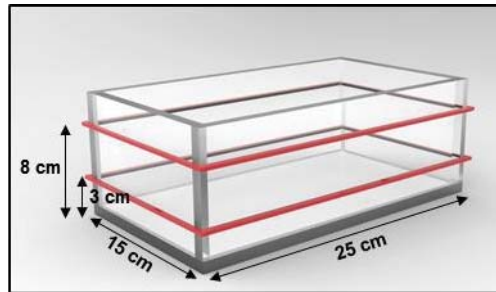


Fig. S11. Scheme of the experimental arena circumflexed with antenna for wireless power supply. The arena has dimensions ($L \times W \times H = 25 \times 15 \times 10$ cm) similar to a regular mouse home cage and is circumflexed with a dual loop antenna (indicated by red lines).

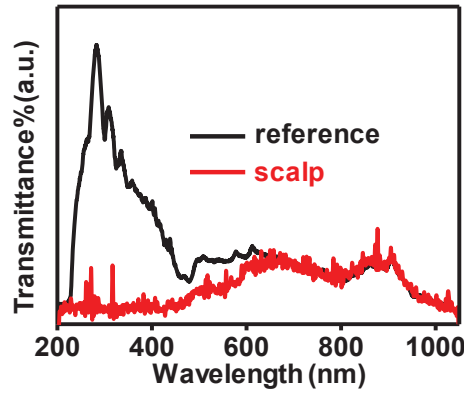


Fig. S12. Transmittance spectra of mouse scalp collected by a fiber optic spectrometer. The sample (labelled as “scalp”) is enclosed in a plastic container and the plastic container serves as the “reference”. The integration time for the measurements is set to keep the recorded transmittance of scalp and reference samples the same in the spectral band of ~700–1000 nm.

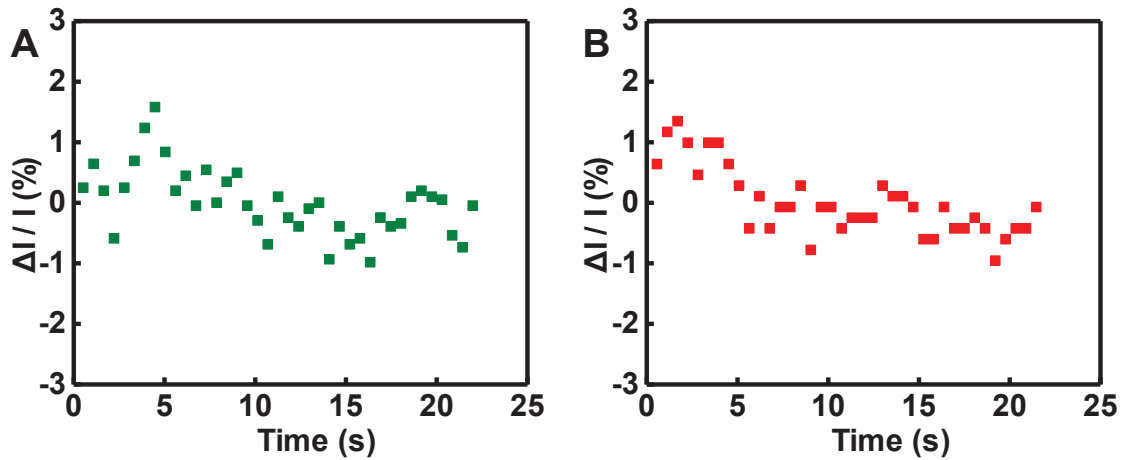


Fig. S13. Fluctuations in output signals ($\Delta I/I$) of the wireless, battery-free oximeters over time. The fluctuation in output signals is defined as the variance between each recorded ADC value and the mean value, divided by the mean value. (A) and (B) show data related to green and red μ -ILEDs, respectively. The probe of wireless oximeters is immersed in solution 1 (commercial hemoglobin powder dissolved in PBS buffers, 25 g/L) placed in an experimental arena with the dimensions of a mouse home cage and with the RF power input of 4 W.

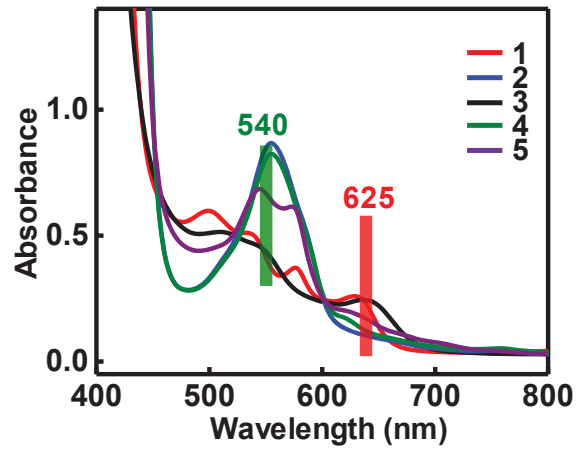


Fig. S14. Absorption spectra of five artificial blood solutions with various combinations of oxyhemoglobin, deoxyhemoglobin, and metHb. The concentration of total hemoglobin in each solution for the UV-visible spectroscopic measurements is 1.25 g/L. The green and red bars indicate the dominant emission wavelengths of the green (540 nm) and red (625 nm) μ -ILEDs.

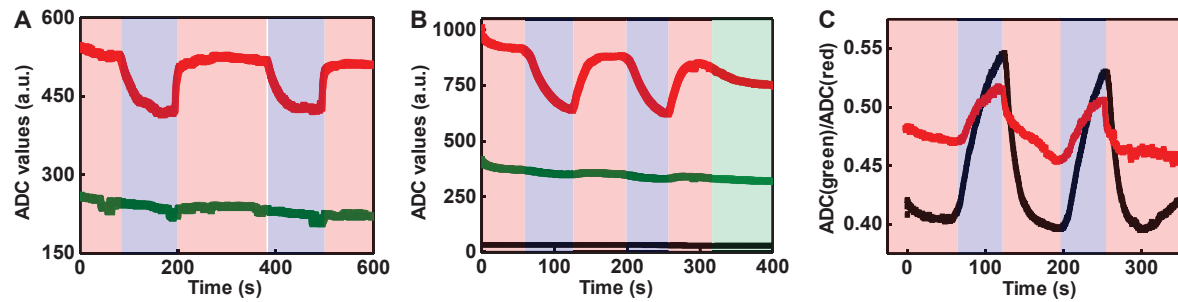


Fig. S15. Raw data of rStO₂ collected by wireless, battery-powered oximetry implants in the tissue region near femoral artery of anesthetized rats. (A, B) Temporal changes in raw ADC values of output photoresponses related to green (green curves) and red (red curves) μ -ILEDs in response to FiO₂ challenges. The black curve in (B) corresponds to baseline data (related to the dark current of the μ -IPD) recorded when both μ -ILEDs are off. **(C)** Changes in the ratio of ADC values associated with green and red μ -ILEDs when implanting the device right underneath the femoral artery (0.5–1 mm, black curve) and in deep tissue (2–4 mm, red curve), highlighting the sensing capability of highly localized rStO₂. For all experiments, the rats are exposed to different FiO₂ though a nose cone (red blocks: hyperoxia: pure O₂ with 2% isoflurane; purple blocks: hypoxia: 8% O₂; green blocks: normoxia: ambient atmosphere).

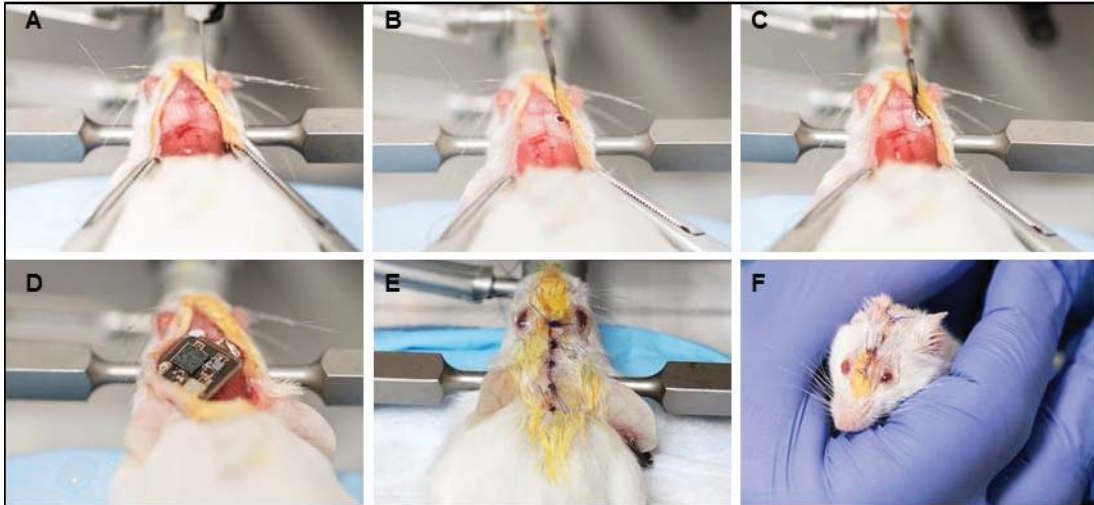


Fig. S16. Surgical steps of the subdermal implantation of wireless, battery-free oximeters in mouse brain. (A) Fixing the head of an anesthetized mouse on the stereotax followed by scalp opening. (B) Opening a hole with a drill bit in the skull for filament implantation. (C) Lowering the injectable filament into the hole and fixing it with dental cement or cyanoacrylate. (D) Bending the electronic module and laying it on the skull. (E, F) Closing scalp with bioresorbable sutures. (Photo credit: Philipp Gutruf, Northwestern University)

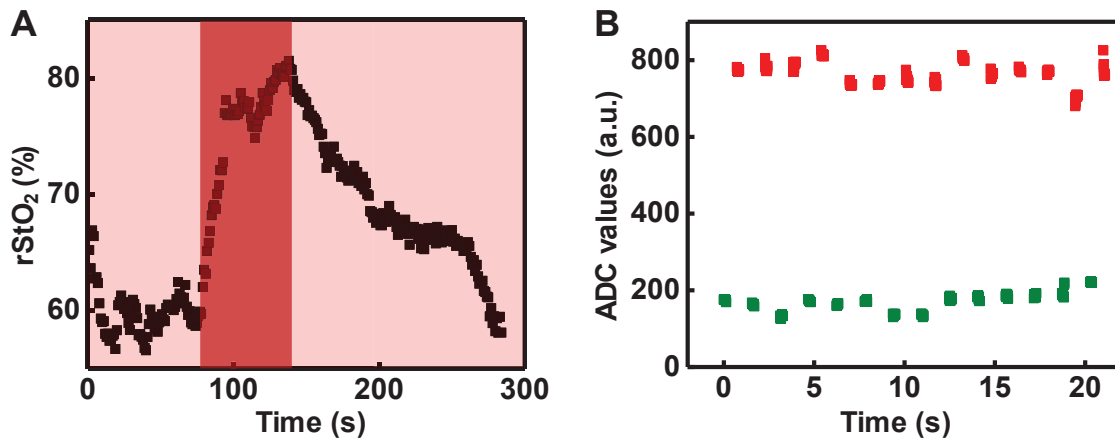


Fig. S17. Wireless oximetry data on mice with subdermally implanted, battery-free devices in the brain. (A) Temporal changes in estimated rStO₂ of an anesthetized mouse experiencing normal anesthesia gas mixture (O₂ with 2% isoflurane, indicated by light red blocks) or increased flow rates of O₂ supply (indicated by dark red block) via a nose cone; **(B)** Temporal raw ADC values of output photoresponses related to green (green squares) and red (red squares) wavelengths from subdermal, wireless oximetry implants in a freely-moving mouse at ambient atmosphere.

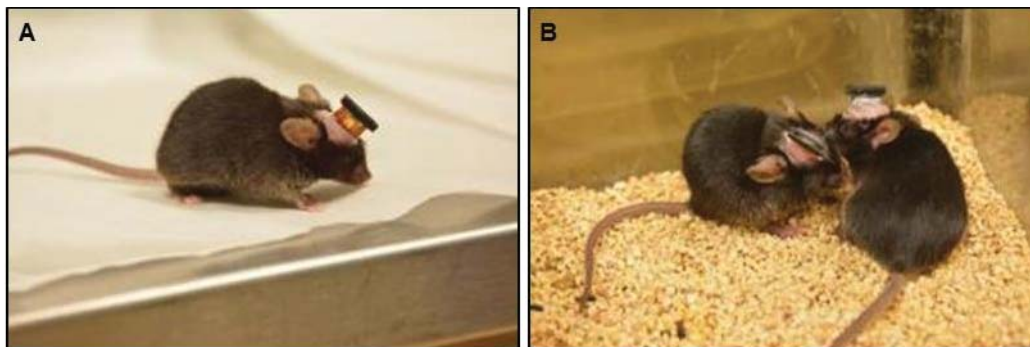


Fig. S18. Photographs of freely moving mice with brain-implanted oximeter filaments with connectors for the integration with battery-powered electronics. (Photo credit: Michael C. Montana, Washington University School of Medicine)

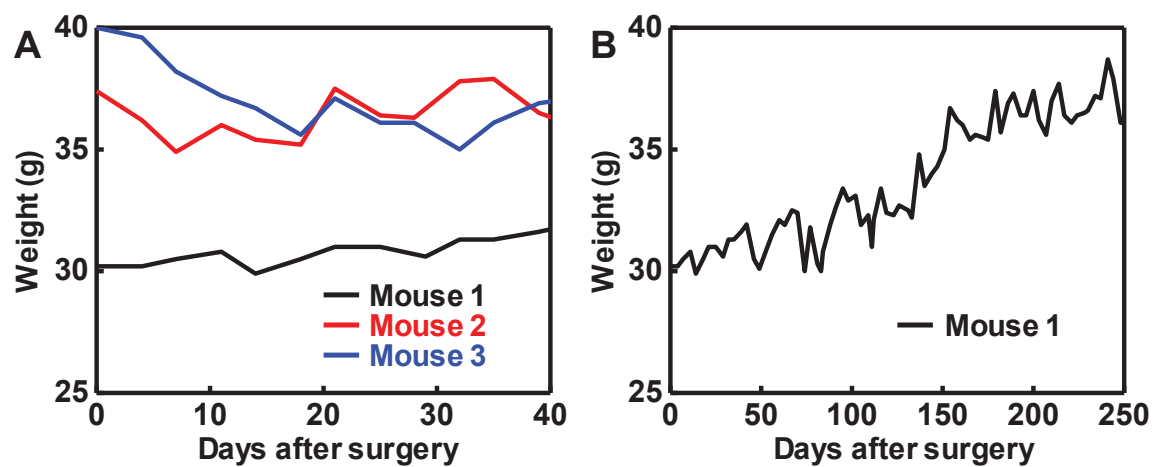


Fig. S19. Weight changes of three mice after subdermal brain surgery with wireless, battery-free oximetry implants.

Table S1. Data transmission of the wireless, battery-free oximeters before and after subdermal implantation. Encoding: NEC, Code: 0 (12 bits), Sequential timing with timing tolerance of 50 μ s. Numbers in red and black colors correspond to ON and OFF states.

Timing before implantation (μ s)	Timing after implantation (μ s)
8850	8800
4350	4350
600	650
500	500
600	550
500	550
650	650
500	500
600	600
500	500
650	650
450	500
650	600
500	550
600	600
500	500
650	600
500	500

600	600
500	500
600	600
500	550
650	600
500	500
600	650
500	500
650	600

Movie S1. A wireless, battery-free, fully implantable oximeter with illuminating μ -ILEDs.

(Movie Credit: Philipp Gutruf, Northwestern University)